ACSNANO

www.acsnano.org

ARTICLE

Tuning the Glass Transition: Enhanced Crystallization of the Laves Phases in Nearly Hard Spheres

Tonnishtha Dasgupta,[‡] Gabriele M. Coli,[*,‡] and Marjolein Dijkstra

Cite This: *ACS Nano* 2020, 14, 3957−3968

Read Online

ACCESS | Metrics & More | Article Recommendations | Supporting Information

ABSTRACT: **Colloidal crystals with a diamond and pyrochlore structure display wide photonic band gaps at low refractive index contrasts. However, these low-coordinated and open structures are notoriously difficult to self-assemble from colloids interacting with simple pair interactions. To circumvent these problems, one can self-assemble both structures in a closely packed $MgCu_2$ Laves phase from a binary mixture of colloidal spheres and then selectively remove one of the sublattices. Although Laves phases have been proven to be stable in a binary hard-sphere system, they have never been observed to spontaneously crystallize in such a fluid mixture in simulations nor in experiments of micron-sized hard spheres due to slow dynamics. Here we demonstrate, using computer simulations, that softness in the interparticle potential suppresses the degree of 5-fold symmetry in the binary fluid phase and enhances crystallization of Laves phases in nearly hard spheres.**

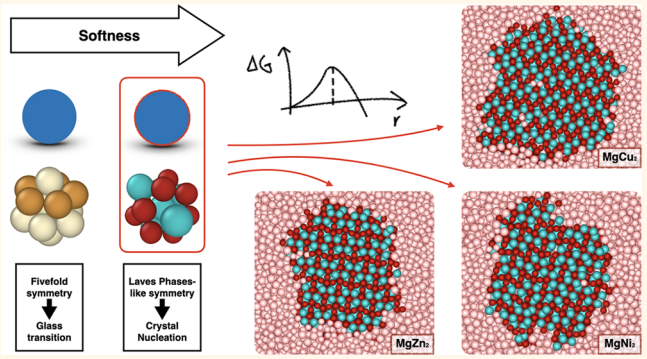

KEYWORDS: *colloidal particles, Laves phases, Monte Carlo methods, glass transition, 5-fold symmetry, photonic crystals*

Photonic crystals (PCs) are periodic dielectric structures that possess a photonic band gap that forbids the propagation of light at certain frequency ranges. The ability to control the flow of light is attractive for numerous applications, ranging from lossless dielectric mirrors, bending of light around sharp corners in optical waveguides, and telecommunications, to optical transistors in optical computers. A highly promising route to fabricate photonic crystals is *via* self-assembly of optical wavelength sized colloidal building blocks. PCs that display a wide omnidirectional photonic band gap at low refractive index contrasts are related to the family of either the diamond or the pyrochlore structure. However, these low-coordinated crystals are notoriously difficult to self-assemble from colloids with simple isotropic pair interactions.

One strategy to form open lattices is by employing long-range Coulomb interactions with a range that exceeds multiple times the particle size.[1,2] The range of the screened Coulomb interaction is set by the Debye screening length of the solvent, like water or other polar solvents, which is why this approach will fail for particle sizes that are required for opening up a photonic band gap in the visible region.

To circumvent these problems associated with the self-assembly of low-coordinated crystal structures, one can also employ a different route in which both the diamond and pyrochlore structure are self-assembled in a single close-packed $MgCu_2$ crystal structure from a binary colloidal dispersion. By selectively removing one of the species, one can obtain either the diamond (Mg, large spheres) or the pyrochlore (Cu, small spheres) structure. $MgCu_2$ is one of the three *binary* LS_2 crystal structures (L = large species, S = small species), also known as Laves phases (LPs), as first found in intermetallic compounds. The three main structural prototypes of the LPs are the hexagonal $MgZn_2$, cubic $MgCu_2$, and hexagonal $MgNi_2$ structures, which can be distinguished by the stacking of the large-sphere dimers in the crystal structures (Figure 1). Experimentally, LPs have been observed in binary nanoparticle suspensions[3,4] and in sub-micron-sized spheres interacting *via* soft repulsive potentials.[5−10]

Received: September 6, 2019
Accepted: April 6, 2020
Published: April 6, 2020

https://dx.doi.org/10.1021/acsnano.9b07090
ACS Nano 2020, 14, 3957−3968

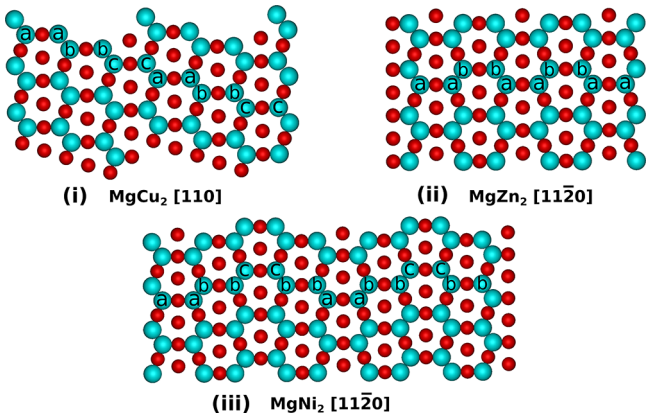

Figure 1. Structure of the three types of Laves phases, showing the different stacking sequences of the large-sphere dimers, marked as "aa", "bb", and "cc", when viewed along specific projection planes. The stacking of the large-sphere dimers is (i) "··· aa-bb-cc···" for $MgCu_2$, (ii) "··· aa-bb···" for $MgZn_2$, and (iii) "··· aa-bb-cc-bb···" for $MgNi_2$.

Although free-energy calculations in Monte Carlo (MC) simulations have demonstrated that the LPs are thermodynamically stable for a binary hard-sphere (BHS) mixture with a diameter ratio of $0.76 \leq q = \sigma_S/\sigma_L \leq 0.84$,[11] LPs have never been observed to spontaneously crystallize in such a binary fluid mixture in computer simulations (after the submission of the paper, a preprint was submitted in which the spontaneous formation of LPs was reported in simulations, but this proceeds *via* spinodal decomposition).[12] There are numerous possible reasons. First of all, it may be possible that the LPs are not stable in such a hard-sphere mixture and should be replaced by a crystal structure that has been ignored so far in phase diagram calculations.[11] Second, the freezing transition of the LPs in a BHS fluid is located at very high densities. Nucleation can thus only occur when the system is sufficiently dense. At these high concentrations, nucleation is severely hampered by slow dynamics. Binary mixtures with a diameter ratio of $q \approx 0.8$, identical to the range where the LPs are stable, are known to be excellent glass formers.[13] This, in conjunction with the above factor, makes the self-assembly of LPs in BHS mixtures an extremely rare event. Furthermore, due to small free-energy differences, the three LPs are strongly competing during the crystallization process, leading to numerous stacking faults in the final crystal structure.[14−17]

The suppression of crystallization due to glassy behavior is often rationalized by the prevalence of icosahedral clusters of spheres whose short-range 5-fold symmetry is incompatible with the long-range translational order as exhibited by crystals.[18] The icosahedral order arises when one maximizes the density, using the convex hull, of a packing of 12 identical spheres in contact with a central sphere of the same size. The densest packing is obtained by arranging the outer spheres on the vertices of an icosahedron, rather than by using 13-sphere subunits of face-centered cubic and hexagonal close-packed bulk crystals.

Here we demonstrate that spontaneous crystallization of the LPs is strongly suppressed by the presence of 5-fold symmetry structures in a binary fluid of hard spheres. Interestingly, we show that softness of the interaction potential reduces the degree of 5-fold symmetry in the binary fluid phase. We systematically study the role of softness in the interaction potential on the structure, phase behavior, and nucleation of the LPs. By carefully tuning the particle softness, we observe for the first time spontaneous nucleation of the LPs in a nearly hard-sphere system in computer simulations, thereby providing evidence that the LPs are stable in a binary hard-sphere system. The key result of this study is that soft repulsive spheres can be mapped onto a hard-sphere system in such a way that the structure and thermodynamics are invariant, but that the dynamics and therefore the kinetic glass transition are strongly affected by higher-body correlations, *i.e.*, 5-fold symmetry clusters, which can be tuned both in simulations and in experiments by the softness of the particle interactions. In this way, softness suppresses 5-fold symmetry and enhances crystallization of the LPs.

This work is organized as follows. In the section Freezing Transition and 5-fold Symmetry, we detemine the binary fluid−LP phase coexistence for a BHS mixture and a Weeks−Chandler−Andersen (WCA) mixture for varying degrees of softness in the interaction potentials. We find that the freezing transition shifts to higher number densities with increasing particle softness. As crystallization may be suppressed by slow dynamics due to the presence of 5-fold symmetry clusters, we investigate the number fraction of 5-fold symmetry clusters as a function of supersaturation. Surprisingly, we find that a tiny softness in the interparticle potential is able to reduce the fraction of 5-fold symmetry clusters that are responsible for the slow dynamics in the fluid phase.

This interesting finding immediately begs the question whether or not LP nucleation can be observed by particle softness. To this end, we study nucleation of the LP using the seeding approach for varying particle softness in the section Nucleation Behavior. We find a significant collapse of the nucleation barrier heights and rates as a function of supersaturation for the three different LPs and varying particle softness. Pinpointing the supersaturation range where the nucleation barrier becomes very low enables us to observe for the first time spontaneous nucleation of the LP as reported in the section Spontaneous Nucleation. Moreover, we find that the supersaturation level where the fluid becomes unstable with respect to the LP is universal for all WCA systems.

We then continue by investigating the thermodynamic invariance of the WCA systems by relating the thermodynamics and structural two-body correlations to that of the hard-sphere system in section Invariance with Hard Spheres.

Finally, in the section Kinetic Glass Transition, we measure in simulations the structural relaxation time as a function of density and fit our data with a prediction from mode-coupling theory to estimate the kinetic glass transition. We find that the kinetic glass transition depends strongly on particle softness. For the lowest softness and therefore also for BHS, we find that the glass transition pre-empts the packing fraction where the fluid becomes unstable with respect to the LP, in contrast to the softer WCA systems. Intriguingly, we also find a marked correlation between the relaxation times and the fraction of 5-fold symmetric clusters calculated in the first section.

RESULTS AND DISCUSSION

Freezing Transition and 5-fold Symmetry. *Phase Diagram Calculation.* We first study the effect of particle softness on the freezing transition of the LPs in a binary fluid of soft repulsive spheres. To vary the softness of the pair interaction, we consider a binary mixture of N_L large (L) and N_S small (S) spheres in a volume V interacting with a WCA potential $u_{\alpha\beta}(r_{ij})$ between species $\alpha = L, S$ and $\beta = L, S$[19]

https://dx.doi.org/10.1021/acsnano.9b07090
ACS Nano 2020, 14, 3957−3968

$$u_{\alpha\beta}(r_{ij}) = 4\epsilon\left[\left(\frac{\sigma_{\alpha\beta}}{r_{ij}}\right)^{12} - \left(\frac{\sigma_{\alpha\beta}}{r_{ij}}\right)^{6} + \frac{1}{4}\right] \quad r_{ij} < 2^{1/6}\sigma_{\alpha\beta}$$
$$= 0 \quad r_{ij} \geq 2^{1/6}\sigma_{\alpha\beta} \tag{1}$$

where $r_{ij} = |\boldsymbol{r}_i - \boldsymbol{r}_j|$ denotes the center-of-mass distance between particles i and j, $\boldsymbol{r}_i$ the position of particle i, and ϵ the interaction strength. For a BHS mixture, LPs are thermodynamically stable for a diameter ratio $q \in [0.76, 0.84]$.[11] In this work, we set the diameter ratio $q = \sigma_S/\sigma_L = 0.78$, which is close to the value of a recent experimental study.[20] Here σ_α denotes the diameter of species α and $\sigma_{\alpha\beta} = (\sigma_\alpha + \sigma_\beta)/2$. The *softness* of the potential can be tuned by changing the reduced temperature $T^* = k_BT/\epsilon$ with k_B being Boltzmann's constant and T the temperature. The WCA potential has been previously used to mimic the interactions between hard spheres[21−24] as it reduces to the hard-sphere potential in the limit of $T^* \to 0$. In Figure 2, we plot the WCA potential for T^*

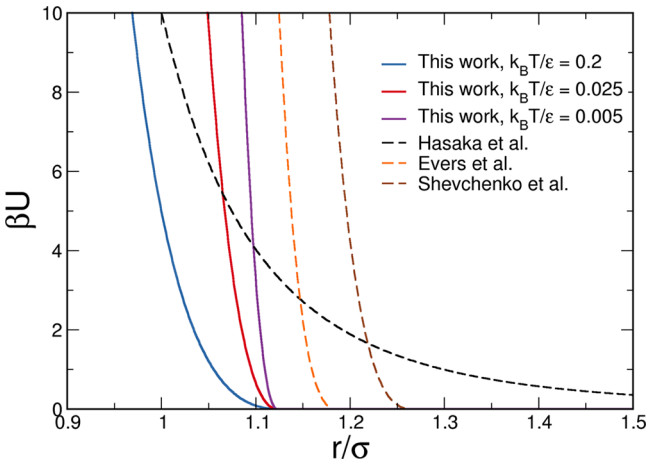

Figure 2. WCA potential at $T^* = k_BT/\epsilon$ = 0.2, 0.025, and 0.005 along with the pair potentials of the experimental systems (dashed lines) for which the Laves phase has been reported in the literature, which are binary nanoparticle suspensions of Evers *et al.*[4] and Shevchenko *et al.*,[3] and polystyrene spheres of Hasaka *et al.*[6]

= 0.005, 0.025, and 0.2 along with the pair potentials of some notable experimental systems for which the Laves phases have been reported in the literature, which are polystyrene latex spheres[6] and binary nanoparticle suspensions.[3,4] Figure 2 shows that the WCA potential at $T^* = 0.025$ agrees well with that of the nanoparticle systems of Evers *et al.*[4] and Shevchenko *et al.*,[3] whereas the WCA potential at $T^* = 0.2$ is slightly softer. The pair potential of the polystyrene latex spheres of Hasaka *et al.*[6] is considerably softer and more long ranged than the WCA pair interactions used in the present study.

We first determine the freezing transition of the LPs for varying softness of the interparticle potential using thermodynamic integration of the equation of state of the binary fluid phase at a composition $x_L = N_L/(N_L + N_S) = 1/3$, corresponding to the stoichiometry of the LPs and an Einstein integration for the LPs to obtain the free energies of the fluid and LPs, respectively. A more detailed description can be found in the Supporting Information. By employing a common-tangent construction on the free-energy curves, we obtain the fluid−LP coexistence, which is plotted in Figure 3 in

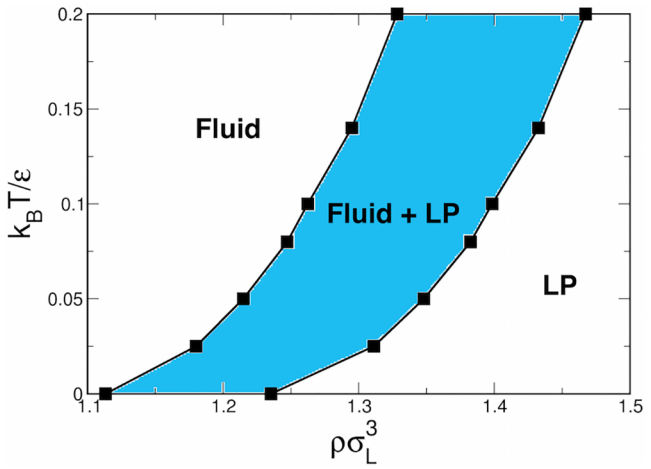

Figure 3. Fluid−Laves phase (LP) coexistence as denoted by the blue region of a binary mixture of WCA spheres with a diameter ratio q = 0.78 at a fixed composition $x_L = N_L/(N_L + N_S) = 1/3$ in the reduced temperature k_BT/ϵ−reduced density $\rho\sigma_L^3$ plane. In the limit of $k_BT/\epsilon \to 0$, the system reduces to a binary mixture of hard spheres.

the temperature k_BT/ϵ−reduced density $\rho\sigma_L^3$ plane, where $\rho = (N_L + N_S)/V$ denotes the density. We find that the freezing transition moves to higher $\rho\sigma_L^3$ with increasing temperature or softness of the particle interaction.

The bulk densities of the fluid−LP coexistence for a BHS mixture with a diameter ratio $q = 0.78$ correspond to packing fractions $\eta_{BHS}^{(f)} = 0.5356$ and $\eta_{BHS}^{(LP)} = 0.5943$ for the fluid and LP, respectively. As the freezing transition of the LPs is located at relatively high densities, crystallization is likely suppressed by slow dynamics.

High-Coordination Clusters. In the case of monodisperse spheres, glassy dynamics and suppression of crystallization are often linked to the presence of icosahedral clusters with 5-fold symmetry in the supersaturated fluid, which is incompatible with the long-range periodic order of a crystal. To investigate whether or not 5-fold symmetry structures suppress crystallization of the LPs in a binary fluid mixture at composition $x_L = 1/3$, we measure the number fraction of three significant representatives of the 5-fold symmetry structures, *i.e.*, the pentagonal bipyramids, defective icosahedra, and regular icosahedral clusters as depicted in Figure 4, using the topological cluster classification (TCC)[25] for varying softness of the interparticle potential. The effect of the presence of these clusters on the kinetics and nucleation of monodisperse hard-sphere systems has already been investigated.[26,27] In order to investigate the effect of particle softness, we compare the number fraction of these clusters at fixed supersaturation $\beta\Delta\mu$ for varying temperatures T^*. The supersaturation $\beta\Delta\mu = \beta\mu_{fluid}(P) - \beta\mu_{LP}(P)$ is defined as the chemical potential difference between the supersaturated fluid and the stable LP at pressure P.

In Figure 4, we plot the number fraction N_c/N of the three investigated clusters in a binary fluid mixture at composition $x_L = 1/3$ *versus* $\beta\Delta\mu$ for varying T^* corresponding to different

https://dx.doi.org/10.1021/acsnano.9b07090
ACS Nano 2020, 14, 3957−3968

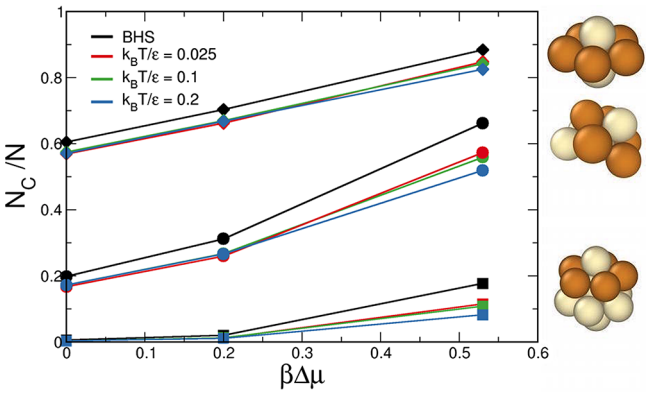

Figure 4. Number fraction of particles N_c/N belonging to three different 5-fold symmetry clusters as a function of the supersaturation $\beta\Delta\mu$ of the fluid phase of a binary mixture of WCA spheres at varying temperatures as labeled corresponding to different degrees of particle softness and of a binary hard-sphere mixture. The three data sets correspond to pentagonal bipyramids (diamonds), defective icosahedra (bullets), and icosahedra (squares). The error bars determined from five independent simulation runs are smaller than the symbols and are presented in Table I in the Supporting Information. Sketches of these clusters are shown on the right. We highlight (one of the) pentagons in the respective clusters.

particle softness. We clearly see that the number fraction of 5-fold symmetry clusters increases with $\beta\Delta\mu$, but more significantly, it decreases substantially with a small increase in particle softness. Notably, the five-membered rings as observed in the clusters highlighted in Figure 4 are also prevalent in the three LP crystal structures. It is thus not immediately clear whether these pentagons in the supersaturated fluid act as nucleation precursors or are responsible for the slow dynamics.

We therefore analyze the five-membered rings further in the BHS fluid phase as well as in the three ideal LPs and classify them according to their large/small sphere composition and topology. In particular, to ensure that the systems at high supersaturation ($\beta\Delta\mu = 0.53$) are well-equilibrated, we run the simulations for a very long time (>10^7 MC cycles). We distinguish eight topologies (indexed $\mathcal{N}$) in Figure 5(b) and measure the probability to observe a specific topology $P(\mathcal{N})$ in the ideal LPs and the metastable BHS fluid at a high supersaturation $\beta\Delta\mu \simeq 0.53$. We reason that if these five-membered rings are formed randomly in a fluid mixture, $P(\mathcal{N})$ should follow a binomial distribution where the probability to observe a large sphere in a pentagonal cluster is determined by the composition x_L. We present the probability distributions $P(\mathcal{N})$ for the LPs, the metastable fluid, and binomial distribution all at a composition $x_L = 1/3$ in Figure 5(a). We find that the probability distribution $P(\mathcal{N})$ of the pentagons in the BHS fluid mixture (black line in Figure 5(a)) and in the WCA mixtures (see the Supporting Information) follows reasonably well the binomial distribution (pink line in Figure 5(a)) for all topologies, demonstrating that the pentagons are formed randomly in the fluid. Furthermore, the pentagons with a topology $\mathcal{N} = 1$ are predominant in the supersaturated BHS fluid phase, whereas pentagons with a topology $\mathcal{N} = 3$ and 4 are prevalent in the ideal LPs. We therefore conclude that the 5-fold symmetry clusters in the supersaturated fluid do not act as precursors for crystallization, but are responsible for the slowing down of the dynamics and the kinetic arrest.

For future studies, it may be interesting to investigate whether a slightly different composition of the mixture, namely, one that increases the probability of finding pentagonal clusters with a topology that is found in LPs, may enhance LP crystallization.[28] More importantly, we find that the presence of these 5-fold symmetry clusters can be reduced significantly by particle softness. This unexpected finding raises the immediate question whether or not crystal nucleation of the LPs can be enhanced or suppressed by tuning the softness of the interparticle potential.

Nucleation Behavior. To investigate the effect of particle softness on the nucleation of the LPs, we determine the nucleation barrier height, critical nucleus size, and nucleation rate using the seeding approach.[29,30] This technique involves inserting a crystalline seed of a predetermined shape and size into a metastable fluid. The configuration is subjected to a two-step equilibration process in the *NPT* ensemble where (i) the interface between the crystalline cluster and surrounding fluid

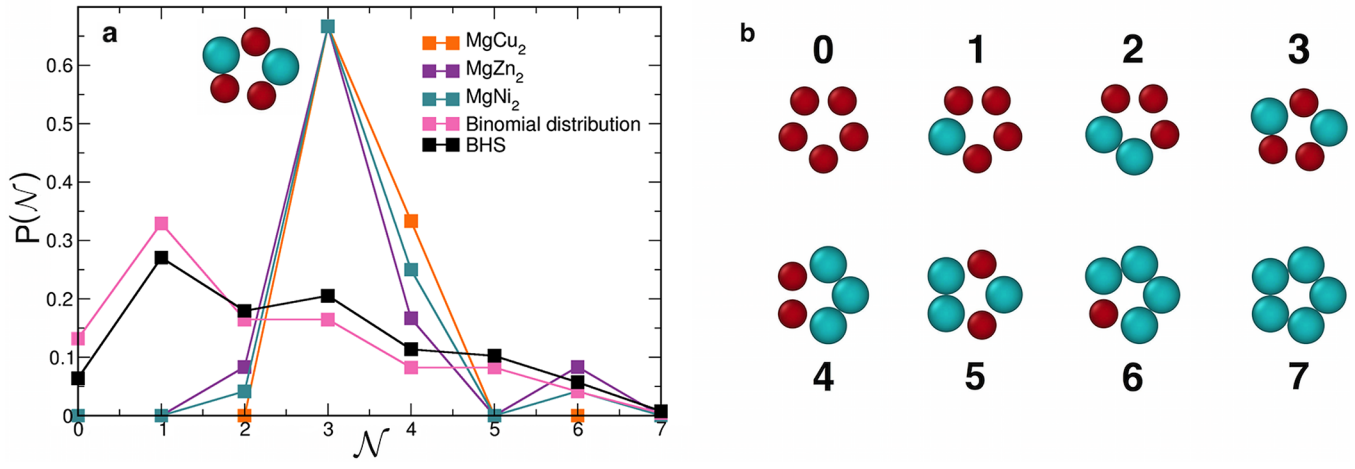

Figure 5. (a) Probability distribution to observe a specific cluster topology $P(\mathcal{N})$ for the five-membered rings for the three ideal LPs, a supersaturated binary hard-sphere (BHS) fluid ($\beta\Delta\mu \simeq 0.533$), and a binomial distribution, all at composition $x_L = 1/3$. The eight distinct cluster topologies are shown in (b) with their index label $\mathcal{N}$. The error bars determined from five independent simulation runs are smaller than the symbols and are presented in Table 2 in the Supporting Information.

https://dx.doi.org/10.1021/acsnano.9b07090
ACS Nano 2020, 14, 3957−3968

is equilibrated by keeping the cluster fixed and then (ii) the constraint on the cluster is relaxed and the system is equilibrated further. Subsequently, the equilibrated configuration is simulated for a range of pressures in order to determine the critical pressure $\beta P_c\sigma_L^3$ at which the critical cluster size of N_c particles stabilizes. We note that seeding simulations in the *NVT* ensemble have a strong dependence on system size due to a progressive depletion of particles in the supersaturated fluid phase when a crystal nucleus starts to grow and due to a drop in pressure when the fluid starts to crystallize. In order to avoid finite-size effects, we perform simulations in the *NPT* ensemble, where the system is subject to a fixed pressure.[23] An illustration is shown in Figure 6,

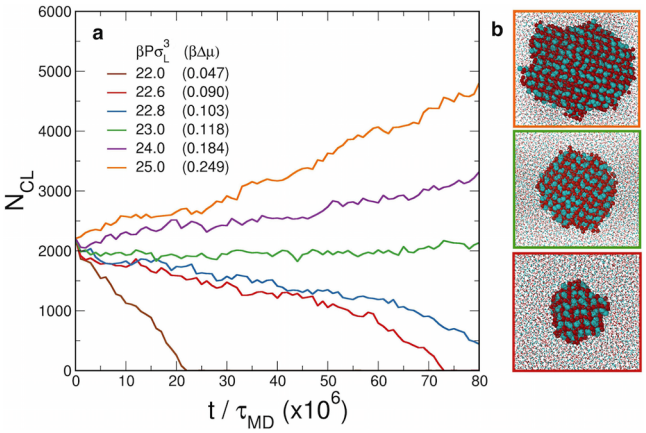

Figure 6. (a) Largest cluster size N_{CL} with LP symmetry as a function of time t/τ_{MD} using the seeding approach in MD simulations of a binary mixture of WCA spheres in the *NPT* ensemble at temperature $T^* = 0.2$, composition $x_L = 1/3$, and a diameter ratio $q = 0.78$ for varying pressures $\beta P\sigma_L^3$ with corresponding supersaturations $\beta\Delta\mu$ between brackets in order to estimate the critical pressure $\beta P_c\sigma_L^3$. The initial seed size is 2205 particles of the $MgZn_2$ Laves phase. The snapshots in (b) show the melting of the seed at $\beta P\sigma_L^3 = 22.6$ (red box), growth of the seed at $\beta P\sigma_L^3 = 25$ (orange box), and a stable seed at the critical pressure $\beta P_c\sigma_L^3 = 23$ (green box). The large (small) spheres are colored blue (red). Fluid particles (particles with a disordered neighborhood, see the Supporting Information) are reduced in size for visual clarity.

where a $MgZn_2$ LP seed melts, stabilizes, and grows out, as can be observed from the evolution of the size of the largest cluster N_{Cl} as a function of time t/τ_{MD}, at $\beta P\sigma_L^3 = 22.6$ (red curve), 23 (green), and 25 (orange), respectively. Here, $\tau_{MD} = \sigma_L\sqrt{m/k_BT}$ denotes the MD time unit and m the mass of the particles.

In order to discriminate crystalline clusters with LP-like symmetry from the fluid phase, we use a local bond-orientational order parameter measuring the hexagonal symmetry of every particle i with identity $\alpha(i) \in L, S$. We then determine large−large, large−small, and small−small particle pairs with strongly correlated LP-like symmetry and construct clusters of mutually bonded LP-like solid particles. A detailed description can be found in the Supporting Information.

The height of the Gibbs free-energy barrier ΔG_c for a critical nucleus size N_c can subsequently be obtained from classical nucleation theory:

$$\beta\Delta G_c(N_c) = N_c\beta\Delta\mu/2 \tag{2}$$

By using different critical cluster sizes N_c in the seeding approach, we obtain ΔG_c for varying critical pressures, corresponding to different supersaturations $\beta\Delta\mu$. We repeat these calculations for the three distinct LPs, $MgZn_2$, $MgCu_2$, and $MgNi_2$, as crystalline seeds in the seeding approach. In Figure 7(a), we present ΔG_c as a function of $\beta\Delta\mu$ for the three LPs and for temperatures $k_BT/\epsilon = 0.005$, 0.025, 0.1, and 0.2, corresponding to varying particle softness. We observe that for all temperatures and the three LP types, ΔG_c goes to infinity upon approaching bulk coexistence at $\beta\Delta\mu = 0$, decreases with increasing supersaturation $\beta\Delta\mu$, and approaches zero at sufficiently high $\beta\Delta\mu$. We find that all our ΔG_c data coincide within statistical error bars for all three LPs, which is to be expected, as the free-energy differences between the three bulk LPs are extremely small. More interestingly, we observe that the ΔG_c data collapses onto a master curve for all four temperatures, yielding an intriguing thermodynamic invariance for the different degrees of softness in the WCA interaction potential.

In addition, we calculate the nucleation rate J, which is determined by a thermodynamic term related to the Gibbs free-energy barrier $\beta\Delta G_c$ and a kinetic prefactor:

$$\frac{J\sigma_L^5}{D_L} = \sqrt{\frac{\beta\Delta\mu}{6\pi N_c}}\frac{f^+\sigma_L^2}{D_L}\rho_f\sigma_L^3\exp(-\beta\Delta G_c) \tag{3}$$

where $f^+ = \langle(N(t) - N_c)^2\rangle/t$ is the attachment rate of particles to the critical cluster, t is the time, $\rho_f(\beta P_c\sigma_L^3)$ is the critical density of the fluid at the critical pressure, and D_L is the long-time diffusion coefficient at the same ρ_f. The attachment rate f^+ is measured from 10 independent simulation trajectories at the critical density ρ_f. We present the nucleation rates as a function of $\beta\Delta\mu$ in Figure 7(b) and find that they collapse for all four temperatures and three LPs onto a master curve, in a similar way to what we observed for the nucleation barriers in Figure 7(a). This finding can be rationalized by the fact that the nucleation rate is predominantly determined by the thermodynamic term and simply echoes the thermodynamic invariance as observed for $\beta\Delta G_c$ for the three LPs and the four temperatures.

To summarize, we find by employing the seeding approach that both the nucleation barriers and nucleation rates collapse onto a master curve for the different degrees of particle softness and for the three different types of LPs. This finding is in contrast to a previous simulation study that showed that the enhanced crystal nucleation rate for softer spheres is caused by a lower nucleation barrier.[31] Moreover, we find not only that the nucleation barrier decreases with supersaturation $\beta\Delta\mu$ but more importantly this method also allows us to pinpoint the supersaturation range, where the nucleation barrier of the LP becomes so low (less than several k_BT) that spontaneous nucleation should occur.

Spontaneous Nucleation. Guided by the seeding approach results, we perform MD simulations in the *NPT* ensemble and search for spontaneous nucleation of the LP in a highly supersaturated binary fluid phase of soft repulsive spheres, which has hitherto never been observed in previous

https://dx.doi.org/10.1021/acsnano.9b07090
ACS Nano 2020, 14, 3957−3968

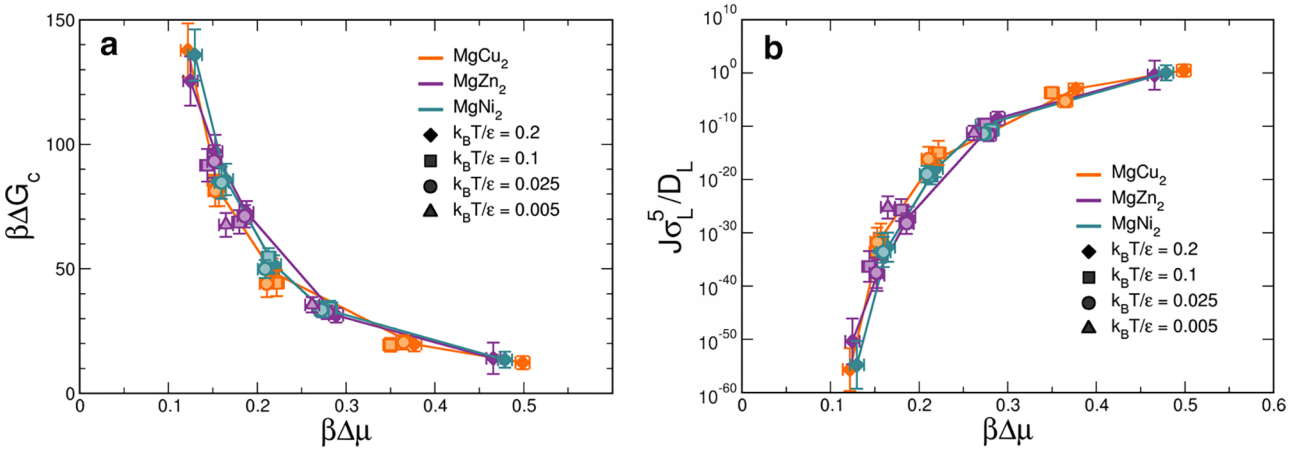

Figure 7. (a) Height of the Gibbs free-energy barrier $\beta\Delta G_c$ and (b) the nucleation rate $J\sigma_L^5/D_L$ as a function of the chemical potential difference $\beta\Delta\mu$ between the fluid and the LP for a binary WCA mixture for the three different LPs and for temperatures k_BT/ϵ = 0.005, 0.025, 0.1, and 0.2.

simulation studies. In Figure 8, we determine the size of the largest cluster N_{CL} with LP symmetry as a function of time t/τ_{MD} for a range of pressures beyond coexistence, for k_BT/ϵ = 0.2, where the coexistence pressure $\beta P\sigma_L^3$ = 21.32. The results yield some interesting observations. At pressure $\beta P\sigma_L^3$ = 29, no crystallization is observed within our long simulation times. At a slightly higher pressure, $\beta P\sigma_L^3$ = 29.5 ($\beta\Delta\mu$ = 0.524), we observe that the system stays in a metastable fluid phase for a certain induction time until a nucleation event occurs; that is, a crystalline nucleus of the $MgZn_2$ phase forms that subsequently grows out and transforms into the $MgCu_2$ phase as soon as the cluster spans the whole simulation box. Upon increasing the pressure further, $\beta P\sigma_L^3 \geq 30$, the crystallization exhibits features of spinodal-like behavior as the supersaturated fluid is unstable with respect to the crystal phase and small crystalline nuclei appear immediately throughout the system. We later refer to this spinodal-like behavior as the instability line, which we define as the lowest pressure $\beta P\sigma_L^3$ (or supersaturation $\beta\Delta\mu$) where crystallization sets in immediately as soon as the simulation is started. For still higher pressures, we again see immediate crystallization, but the clusters grow less, which we attribute to glassy behavior.

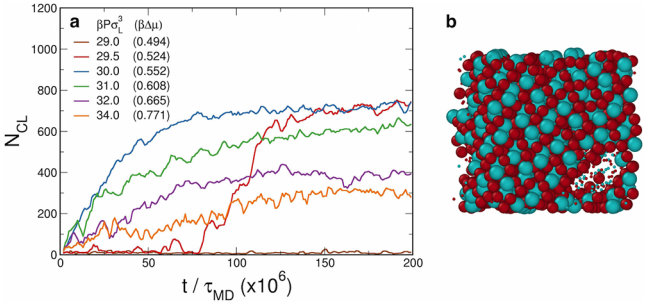

Figure 8. (a) Size of the largest crystalline cluster N_{CL} for a binary mixture of WCA spheres with a diameter ratio q = 0.78 and temperature T^* = 0.2 as a function of time t/τ_{MD} for varying pressures $\beta P\sigma_L^3$ with corresponding supersaturations $\beta\Delta\mu$ between brackets using MD simulations in the *NPT* ensemble. (b) Final configuration of a spontaneous nucleation event at $\beta P\sigma_L^3$ = 29.5 ($\beta\Delta\mu$ = 0.524), initiated by the formation of a crystalline nucleus of the $MgZn_2$ phase that subsequently grows out and transforms into the $MgCu_2$ phase as the cluster spans the simulation box.

More importantly, we also investigate whether or not the nucleation of the LP proceeds *via* a classical pathway by analyzing different particle configurations of a spontaneous nucleation event in time. We observe in the initial stage of the simulation the formation and dissolution of small crystalline nuclei in the binary fluid phase until a crystal nucleus of the LP exceeds its critical size at an intermediate time and subsequently grows out; see the Supporting Information for a movie. We thus show that crystal nucleation of the LP follows a classical pathway. This finding is important, as our approach for estimating the Gibbs free-energy barrier heights and nucleation rates from seeding simulations and classical nucleation theory is only valid in the case that nucleation proceeds *via* a classical nucleation pathway. We hereby validate our method used in the previous section for measuring the nucleation barriers and nucleation rates.

To study the effect of temperature or particle softness on the spontaneous nucleation of the LP in a binary mixture of WCA spheres, we perform MD simulations in the *NPT* ensemble for T^* = 0.1 and 0.025 and pressures higher than the coexistence pressures $\beta P\sigma_L^3$ = 20.03 for T^* = 0.1, and $\beta P\sigma_L^3$ = 18.35 for T^* = 0.025, respectively. We find a similar pressure-dependence (not shown) to that described above for T^* = 0.2: absence of crystallization at low pressures, nucleation in a tiny intermediate pressure regime, and immediate spinodal-like crystallization at $\beta P\sigma_L^3 \simeq$ 27.5 at T^* = 0.1, and $\beta P\sigma_L^3 \simeq$ 25.5 for T^* = 0.025. Surprisingly, the values of the thermodynamic driving force $\beta\Delta\mu$ corresponding to the pressures at which the fluid is unstable are given by $\beta\Delta\mu$ = 0.53 ± 0.02 for all three temperatures, which yields again an intriguing "universality" for the onset of spinodal-like behavior.

Invariance with Hard Spheres. Perturbation and integral equation theories of simple liquids are based on the premise that the structure of monatomic fluids at high densities resembles that of hard spheres.[19,32,33] Hence, a system of hard spheres serves as a natural reference system for determining the properties of more realistic systems. On this basis one expects invariance of the structure along the melting and freezing line of simple fluids and of thermodynamic properties

https://dx.doi.org/10.1021/acsnano.9b07090
ACS Nano 2020, 14, 3957−3968

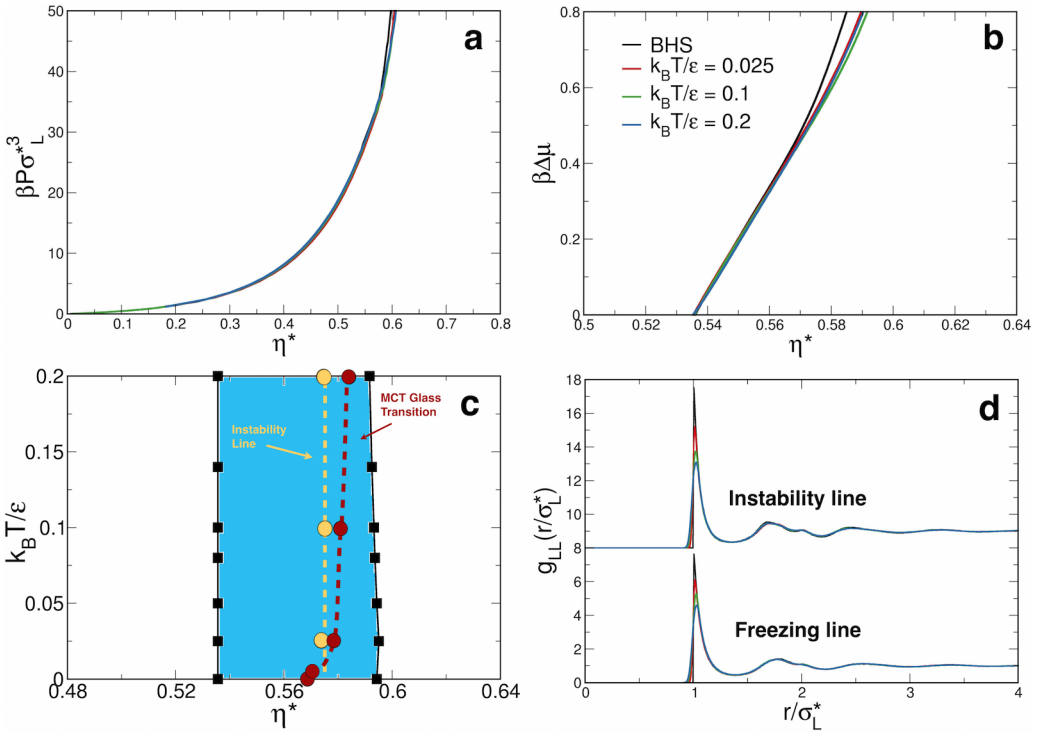

Figure 9. (a) Reduced pressure $\beta P\sigma_L^{*3}$ and (b) supersaturation $\beta\Delta\mu$ *versus* effective packing fraction η^* for a binary hard-sphere mixture and a binary WCA mixture for varying temperatures with a diameter ratio $q = 0.78$ and composition $x_L = 1/3$. The error bars in (a) and (b) are $\lesssim$0.1% and invisible with respect to the line thickness. (c) Phase diagram of this binary WCA mixture in the reduced temperature $k_BT/\epsilon-\eta^*$ plane. The yellow circles connected by a vertical dashed line denote the instability line where the fluid is unstable with respect to freezing. The kinetic MCT glass transition points are denoted by the red circles. For $k_BT/\epsilon = 0.005$, we find that kinetic glass transition precedes the spinodal-like instability, similar to hard spheres. Therefore, the instability point is not marked for this temperature as we do not observe crystallization within reasonable time scales. (d) Pair correlation function $g_{LL}(r)$ for the large spheres as a function of the scaled radial distance r/σ_L^* for a binary mixture of WCA spheres at three different temperatures and for a BHS mixture using MC simulations along the freezing line ($\beta\Delta\mu = 0$) and along the instability line ($\beta\Delta\mu \simeq 0.53$).

such as the relative density change upon freezing and melting.[34,35]

Here, we observe an *invariance* of the Gibbs free-energy barriers, nucleation rates, and the onset of spinodal-like behavior as a function of $\beta\Delta\mu$ for binary WCA mixtures at different temperatures. Inspired by this significant observation, we investigate whether other thermodynamic quantities *and* structural properties are invariant along the freezing line of our WCA systems. Such an invariance is very interesting, as it allows us to map the WCA mixture onto a simple binary hard-sphere system. A BHS mixture with a fixed composition depends on only one thermodynamic variable, the overall packing fraction, thereby yielding a simple one-dimensional phase diagram with a singular freezing and melting transition. In addition, the invariance may enable us to make predictions on the nucleation of the LP in a binary hard-sphere mixture and may shed light on why LP nucleation is observed in a binary mixture of soft repulsive spheres and not in a system of hard spheres.

Thermodynamic Invariance. To investigate the thermodynamic invariance of our WCA systems, we relate the thermodynamic properties of the WCA systems to those of a reference hard-sphere system. For this purpose, we scale the freezing number density of the binary WCA system for $q = 0.78$ at temperature T^* to the binary hard-sphere freezing packing fraction $\eta_{BHS}^{(f)}$, which allows us to determine an *effective diameter* σ_L^* as well as an effective packing fraction η^* at each temperature, in a similar way to that in refs 22 and 36. For a BHS mixture with a diameter ratio $q = 0.78$, the freezing packing fraction is $\eta_{BHS}^{(f)} = 0.5356$. In Figure 9(c), we present the phase diagram in the temperature k_BT/ϵ–effective packing fraction η^* plane. As the freezing density for all temperatures of the WCA system is scaled to the freezing density of hard spheres, the freezing line becomes a vertical line in this representation. In addition, we find that the softness of the interactions has only a minor effect on the melting line and the width of the coexistence region. We find that the melting line shifts slightly to lower packing fractions and that the width of the coexistence region decreases marginally upon increasing the softness of the potential, *i.e.*, increasing the reduced temperature T^*. In addition, we also plot the effective packing fractions corresponding to the state points where the fluid becomes unstable with respect to freezing, *i.e.*, $\beta\Delta\mu \simeq 0.53$. This instability line lies well inside the two-phase coexistence region and shifts slightly to higher η^* with increasing temperature T^*.

Subsequently, we use the same effective diameter σ_L^* to scale the equations of state, $\beta P\sigma_L^{*3}$ *versus* η^* for our WCA systems at different temperatures, and compare them with the equation of state for a BHS mixture with a diameter ratio $q = 0.78$. As seen in Figure 9(a), we find a perfect collapse of the equations of state, demonstrating a thermodynamic invariance for the equations of state for the WCA systems with temperature.

https://dx.doi.org/10.1021/acsnano.9b07090
ACS Nano 2020, 14, 3957–3968

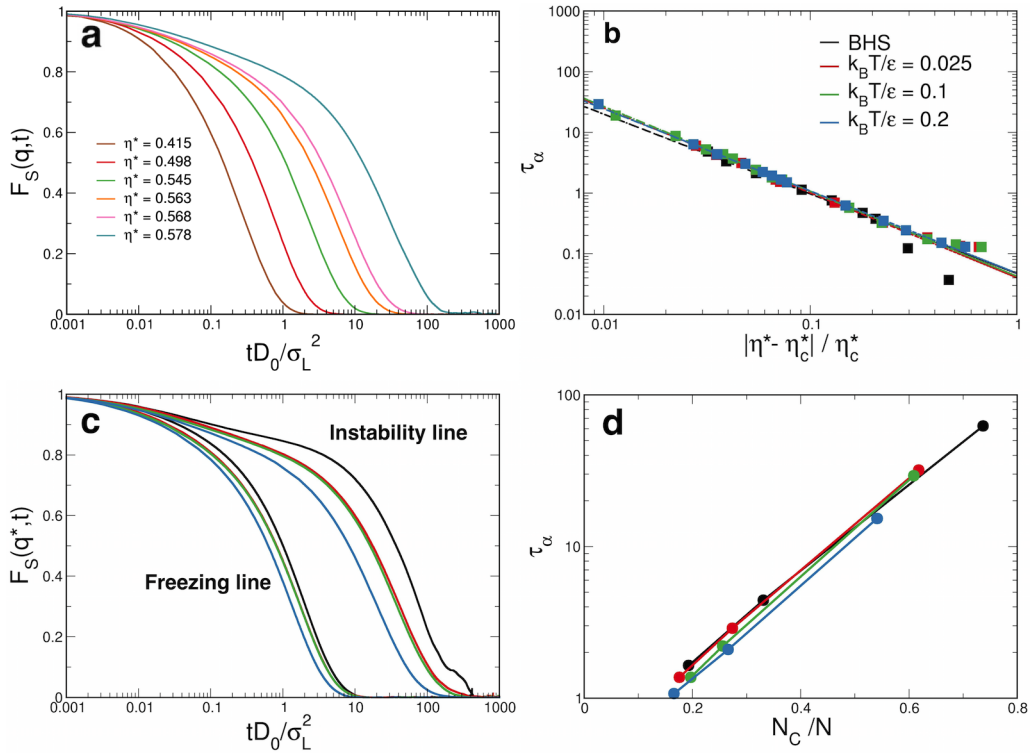

Figure 10. (a) Self-intermediate scattering function $F_s(q, t)$ for the large spheres as a function of time tD_0/σ_L^2 for a binary WCA mixture with a diameter ratio q = 0.78 at T^* = 0.2 for varying effective packing fractions η^* as obtained from MC simulations. (b) Structural relaxation time τ_α as a function of $|\eta^* - \eta_c^*|/\eta_c^*$ for a binary mixture of WCA spheres at T^* = 0.025, 0.1, and 0.2 and a binary hard-sphere mixture. Note that in (c) and (d) the same color coding is used as in (b). (c) Self-intermediate scattering function $F_s(q^*, t)$ for the large spheres for a binary mixture of WCA spheres at three different temperatures and for a BHS mixture using MC simulations along the freezing line and along the instability line. The four curves on the left correspond to $\beta\Delta\mu$ = 0, and the four curves on the right correspond to $\beta\Delta\mu$ = 0.533. (d) Exponential relation between the relaxation time τ_α at three different levels of supercooling ($\beta\Delta\mu$ = 0, $\beta\Delta\mu$ = 0.2, and $\beta\Delta\mu \simeq$ 0.53) and the number fraction of particles N_c/N belonging to a defective icosahedron.

Finally, we plot the chemical potential difference $\beta\Delta\mu = \beta\mu_{\text{fluid}}(P) - \beta\mu_{\text{LP}}(P)$ between the fluid and the Laves phase as a function of the effective packing fraction η^* in Figure 9(b) for both the WCA systems at varying temperatures and the BHS mixture. The deviation of the BHS system from the WCA systems at very high packing fractions $\eta^* \simeq 0.575$ is due to equilibration issues beyond the kinetic glass transition.

The collapse of the chemical potential difference for the WCA systems with different temperatures and the BHS system yields a fascinating "universality" in the thermodynamic driving force for nucleation of the LPs, explaining our observation of the thermodynamic invariance of the Gibbs free-energy barriers, nucleation rates, and the onset of spinodal-like behavior as a function of $\beta\Delta\mu$ for different temperatures as described above. We note that relating the properties of a system with realistic pair interactions to those of a hard-sphere system forms the basis of perturbation theories. The method that we use here to determine the effective diameter of an equivalent hard-sphere system is the simplest one and resembles the expression given by Barker and Henderson.[37] A more accurate prescription is given by the WCA theory, which equates the free energy of the reference system to that of a hard-sphere system at the same density and temperature, yielding a density- and temperature-dependent effective diameter.[38] In lowest order, WCA theory reduces to the Barker–Henderson expression, which is accurate for the WCA systems in the temperature and density range considered here, *i.e.*, $T^* \leq 0.2$ and $\eta^* \leq 0.575$.

Structural Invariance. In order to investigate whether the structure is also invariant along lines in the phase diagrams identified by equal $\beta\Delta\mu$ values, we measure the pair correlation function $g_{LL}(r)$ for the large spheres as a function of the radial distance expressed in terms of the effective diameter of the large spheres for the WCA systems at the three different temperatures and for the BHS mixture along the (i) freezing line $\beta\Delta\mu$ = 0 and (ii) instability line $\beta\Delta\mu \simeq$ 0.53, where we made sure that the system remained in the fluid state during our sampling. The results are presented in Figure 9(d). We find a good collapse of both sets of $g_{LL}(r)$'s as the peak positions coincide, showing a structural invariance of the two-body correlation functions along the freezing and instability lines. Additionally, one observes that the height of the first peak of the $g_{LL}(r)$ increases and the peak becomes narrower, and thus the $g_{LL}(r)$ becomes more hard-sphere-like upon lowering the temperature.

The collapse of the phase diagram, equations of state, and pair correlation functions demonstrate an invariance of the binary WCA mixtures for varying temperatures along lines of equal $\beta\Delta\mu$, *i.e.*, thermodynamic driving force, in the phase diagram. We thus find that a binary mixture of soft repulsive spheres can be mapped onto a hard-sphere system in such a way that the structure and thermodynamics are invariant. However, this invariance does not yet explain why nucleation

https://dx.doi.org/10.1021/acsnano.9b07090
ACS Nano 2020, 14, 3957–3968

of LPs is observed in the case of WCA systems and not for a binary hard-sphere mixture.

Kinetic Glass Transition. To shed light on this counterintuitive result, we investigate the kinetics of the WCA systems as a function of temperature. We already demonstrated above that the degree of 5-fold symmetry clusters can be tuned by the softness of the interaction potential. To investigate the effect of 5-fold clusters on the kinetics of the system further, we determine the kinetic glass transition of the WCA systems at varying temperatures. To this end, we calculate the self-intermediate scattering function $F_s(q, t) = 1/N_L \sum_{j=1}^{N_L} \langle \exp\{i\mathbf{q}\cdot[\mathbf{r}_j(0) - \mathbf{r}_j(t)]\}\rangle$ at the wave vector $q = |\mathbf{q}| = 2\pi/\sigma_L$ as a function of time tD_0/σ_L^2 using MC simulations. The summation runs over all large particles N_L, and the short-time diffusion coefficient of the large spheres D_0 is computed in separate MC simulations. We repeat this calculation for a binary mixture of WCA spheres at temperatures $T^* = 0.2$, 0.1, and 0.025 and for a binary mixture of hard spheres, all at a diameter ratio of $q = 0.78$, using MC simulations at varying effective packing fractions η^*. Exemplarily, we plot $F_s(q, t)$ for a WCA mixture at $T^* = 0.2$ in Figure 10(a) for varying η^*. The dynamics slows down dramatically with increasing η^*. We plot the structural relaxation time τ_α in reduced units, defined by $F_s(q, \tau_\alpha) = e^{-1}$, as a function of $|\eta^* - \eta_c^*|/\eta_c^*$ in Figure 10(b) for our WCA systems at $T^* = 0.025$, 0.1, and 0.2 and the BHS mixture. At sufficiently high densities, the structural relaxation time τ_α diverges algebraically, and we find a perfect collapse of all the data. We employ the prediction from mode coupling theory (MCT),[39] $\tau_\alpha \sim |\eta^* - \eta_c^*|^{-\gamma}$, to fit the structural relaxation times τ_α as a function of η^* using η_c^* and γ as fit parameters. Here, η_c^* denotes the critical packing fraction corresponding to the kinetic glass transition as described by MCT. We note that η_c^* serves solely as a proxy for a qualitative change in the dynamics and mention that for $\eta > \eta_c^*$ the relaxation time diverges exponentially as shown for both active and passive hard-sphere systems.[40,41] The structural relaxation τ_α is well described by an exponential divergence at a packing fraction corresponding to the ideal glass transition as described by the Vogel−Fulcher−Tammann law. We also stress that the structural relaxation times are determined here from simulations, thereby incorporating all many-body correlations in the binary fluid phase in contrast to theoretical predictions from MCT that uses the structure factor (two-body correlation) as input.

We list the critical MCT packing fractions η_c^* with the corresponding supersaturation $\beta\Delta\mu$, critical exponents γ, and the effective diameters σ_L^* in Table 1 for the WCA systems at varying temperatures, *i.e.*, softness of the interaction potential and the BHS mixture. The statistical error on γ (<3%) and η_c^* (<0.2%) are determined by the fit, and on τ_α (<0.1%) by the real part of the $F_s(q, t)$). We also plot the critical MCT packing fractions η_c^* in Figure 9(c). The results are noteworthy. We clearly observe that the critical MCT effective packing fraction η_c^* and corresponding supersaturation $\beta\Delta\mu$ decrease with decreasing softness of the interaction potential. In fact, in the BHS case, the kinetic glass transition, as predicted by MCT, precedes the state point where the fluid becomes unstable with respect to freezing.

Table 1. Critical MCT Effective Packing Fraction η_c^* Corresponding to the Kinetic Glass Transition for a Binary Mixture of WCA Spheres at Varying Temperatures and for a BHS Mixture, All at a Diameter Ratio $q = 0.78$, the Corresponding Supersaturation Level $\beta\Delta\mu$, the Critical Exponents γ of the MCT Fits, and the Effective Large-Sphere Diameters σ_L^*

system	η_c^*	$\beta\Delta\mu$	γ	σ_L^*
$k_BT/\epsilon = 0.2$	0.5837	0.673	1.3545	1.0583
$k_BT/\epsilon = 0.1$	0.5816	0.620	1.3984	1.0764
$k_BT/\epsilon = 0.025$	0.5792	0.604	1.3993	1.1009
BHS	0.5681	0.452	1.3140	1.0000

In order to make a further comparison between the investigated systems, we compare $F_s(q^*, t)$ at the wave vector $q^* = |\mathbf{q}^*| = 2\pi/\sigma_L^*$, for state points along the freezing line $\beta\Delta\mu = 0$ and along the instability line $\beta\Delta\mu \simeq 0.53$ for a BHS system and WCA systems at $T^* = 0.025$, 0.1, and 0.2, in Figure 10(c). Not only do we observe a different dynamical behavior for varying softness, but we also note a strong correlation between the relaxation times τ_α and the number fraction of 5-fold symmetry defective icosahedron clusters. We display this correlation in Figure 10(d), where we find an exponential relation between the structural relaxation times in the fluid phase for varying particle softness and different supersaturations $\beta\Delta\mu$ and the fraction of particles belonging to a defective icosahedron. Such a correlation between the defective icosahedron and the structural relaxation times was also found for weakly polydisperse hard spheres.[42]

To summarize, we find that a BHS mixture gets kinetically arrested at a lower packing fraction than the packing fraction where we expect to find spontaneous nucleation of the LP. However, for a slightly softer interaction potential, a binary WCA mixture at $T^* = 0.025$, we find the reverse situation, and hence spontaneous nucleation is observed at a packing fraction that is lower than that of the kinetic glass transition. This finding may explain why LP nucleation is never observed in a binary mixture of hard spheres and is observed here for a binary WCA system.

CONCLUSIONS

In 2007, a novel self-assembly route toward a photonic band gap material was proposed in which the diamond and pyrochlore structure are self-assembled from a binary mixture of colloidal hard spheres into a closely packed $MgCu_2$ Laves phase.[11] Despite numerous efforts, spontaneous crystallization of the LPs has never been observed in simulations of BHS mixtures or in experiments on micron-sized colloidal hard spheres, casting doubts on the thermodynamic stability of these crystal structures in binary hard spheres. Recent MC simulations have shown, however, that by introducing size polydispersity, either in a static or dynamic way, and by using unphysical particle swap moves, LPs may be nucleated from a dense hard-sphere fluid.[43,44]

Alternatively, to alleviate problems with the degeneracy of the three competing LPs and with the metastability of the $MgCu_2$ with respect to the $MgZn_2$ phase, one may resort to another self-assembly route in which the $MgCu_2$ phase, stable in the present system, is formed from a binary mixture of

https://dx.doi.org/10.1021/acsnano.9b07090
ACS Nano 2020, 14, 3957−3968

colloidal spheres and preassembled tetrahedral clusters of spheres as shown in both simulations[45] and experiments using DNA-mediated interactions.[46]

To better understand why the nucleation of LP is severely hampered in a binary fluid of hard spheres, we investigated the degree of 5-fold symmetry in the binary fluid phase, as the presence of 5-fold symmetry structures may suppress nucleation. In order to study the effect of softness of the interaction potential, we measured the number fraction of three significant representatives of the 5-fold symmetry structures in a binary fluid of WCA spheres at varying temperatures k_BT/ϵ, thereby altering the softness of the interaction potential. In the limit of $k_BT/\epsilon \rightarrow 0$, this system reduces to the binary hard-sphere system. Surprisingly, we found that particle softness significantly reduces the degree of 5-fold symmetry in the binary fluid phase.

To investigate the repercussions of this finding on LP nucleation, we subsequently performed simulations with a crystalline seed to measure the nucleation barrier and nucleation rate for the three LP types and for varying temperatures, *i.e.*, degrees of particle softness. These results enabled us to study, for the first time, spontaneous nucleation of the LPs in simulations of nearly hard spheres. We thus find that the seeding approach is versatile and robust:[29,30] it enables one to not only determine the nucleation barrier and nucleation rate but also locate the regime in the phase diagram where spontaneous nucleation may occur and provides information on how a crystal nucleus grows and melts.

Our observation of spontaneous nucleation of the LP in a system of soft spheres is important and intriguing for two reasons. On one hand, our simulations provide evidence that the LP is stable in the phase diagram of such a binary mixture, as predicted theoretically more than a decade ago.[11] On the other hand, it immediately begs the question why LP nucleation has never been seen in simulations of BHS mixtures or in experiments on micron-sized colloidal hard spheres despite numerous attempts by many research groups, whereas it nucleates spontaneously with a tiny degree of particle softness.

To address this question, we studied the role of softness in the interaction potential on the structure, phase behavior, and dynamics of the LPs and found that a system of soft repulsive spheres can be mapped onto a binary hard-sphere system in such a way that the structure and thermodynamics are invariant in reduced units for varying softness of the interaction potential. However, the invariance of the nucleation barrier and nucleation rate as a function of supersaturation for varying softness of the potential seems to be at odds with the observation of LP nucleation in WCA systems for $T^* \geq 0.025$ and the absence of it in binary hard spheres.

In order to shed light on this counterintuitive result, we determined the kinetic glass transition by fitting the structural relaxation times as obtained from the self-intermediate scattering functions with an MCT fit for the various WCA systems. Surprisingly, we found that the packing fraction corresponding to the kinetic glass transition strongly depends on the softness of the particle interactions, which in turn affects the presence of 5-fold symmetry clusters in the supersaturated fluid phase. It will be interesting to investigate in future work whether or not there is a connection with previous studies that show that the fragility of a glass can be tuned by particle softness.[47−50] We thus find that crystallization can be enhanced by tuning the softness of the particle interactions, either by charge, ligands, or a stabilizer, in simulations or experiments. This finding is indeed consistent with the experimental observations of the LPs, as they all seem to involve particles interacting with (slightly) soft repulsive interactions.[3−10] Moreover, introducing a small degree of softness in the particle interactions can be exploited in a wealth of other crystallization studies. For instance, there are still many open questions on how and why binary crystal phases nucleate. A systematic study of binary nucleation has been hampered so far by either slow dynamics or finding the right regime in the phase diagram where nucleation may occur.

Finally, we note that the structure as characterized by the two-body correlation functions as well as the thermodynamics which is predominantly determined by also two-body correlations is invariant in reduced units for varying softness of the pair potential. However, the structural relaxation time and the kinetics depend strongly on the presence of 5-fold structures, and thus on higher-body correlations. We hope that this finding will inspire the development of new theories for predicting the kinetic glass transition that take into account higher-body correlations.

METHODS

In the determination of the kinetic glass transition and the degree of 5-fold symmetry clusters at different supersaturations, MC simulations were performed on $N = N_L + N_S = 1200$ particles (WCA spheres and binary hard spheres) with composition $x_L = N_L/(N_L + N_S) = 1/3$, in the *NVT* ensemble involving standard single-particle translation moves. The cluster concentrations are averaged over 100 independent snapshots. Spontaneous nucleation of LPs was observed in MD simulations performed using HOOMD-blue (highly optimized object-oriented many-particle dynamics)[51,52] in the *NPT* ensemble on 1536 WCA spheres at composition $x_L = 1/3$. The temperature T and isotropic pressure P are kept constant via the Martyna−Tobias−Klein (MTK)[53] integrator, with the thermostat and barostat coupling constants $\tau_T = 1.0\ \tau_{MD}$ and $\tau_P = 1.0\ \tau_{MD}$, respectively, where $\tau_{MD} = \sigma_L\sqrt{m/\epsilon}$ is the MD time unit. The time step is set to $\Delta t = 0.004\tau_{MD}$ and the simulations are run for $10^9\tau_{MD}$ time steps, unless otherwise specified. The simulation box is cubic and periodic boundary conditions are applied in all directions.

Differently, in the context of the implementation of the seeding approach, the nucleation free-energy barrier heights and nucleation rates were calculated using a crystal seeding approach involving a two-step equilibration process as described in the main text, *via* MC simulations in the *NPT* ensemble involving isotropic volume scale moves in addition to the particle translation moves. The initial configurations were seeded with all three LP types $MgCu_2$, $MgZn_2$, and $MgNi_2$, surrounded by disordered particles, at overall composition $x_L = 1/3$. The data points on the free-energy barrier height and nucleation rate profiles are obtained from simulations with five different seed sizes (N_{seed}): (i) $N_{seed} = 96$ (all three LPs) and total system size $N = 4140$, (ii) $N_{seed} = 192$ ($MgCu_2$), 384 ($MgZn_2$, $MgNi_2$) and $N = 4160$, (iii) $N_{seed} = 648$ ($MgCu_2$), 1080 ($MgZn_2$), 720 ($MgNi_2$) and $N = 8100$, (iv) $N_{seed} = 1536$ ($MgCu_2$), 1728 ($MgZn_2$), 1440 ($MgNi_2$) and $N = 12500$, and (v) $N_{seed} = 3000$ ($MgCu_2$), 2688 ($MgZn_2$, $MgNi_2$) and $N = 17\,000$ particles, respectively. The critical pressures and attachment rates for the different seed sizes were obtained from MD simulations in the *NPT* ensemble, where the simulations were initialized with the MC-equilibrated configurations. The details of the MD simulations are described above.

Finally, in order to investigate the effect of 5-fold symmetry clusters on crystallization, we require an algorithm that is capable of successfully finding different topological clusters in a metastable fluid. To this aim, we employ the topological cluster classification[25] for varying softness of the interparticle potential. The algorithm is

https://dx.doi.org/10.1021/acsnano.9b07090
ACS Nano 2020, 14, 3957−3968

used regardless of the species of the particles forming the clusters, and the bonds between particles are detected using a modified Voronoi construction method. The free parameter f_c, controlling the amount of asymmetry that a four-membered ring can show before being identified as two three-membered rings, is set to 0.82.

The details on the free-energy calculations and on the local bond-orientational order parameter employed to detect clusters with LP-like symmetry can be found in the Supporting Information.

ASSOCIATED CONTENT

Supporting Information

The Supporting Information is available free of charge at https://pubs.acs.org/doi/10.1021/acsnano.9b07090.

Details about the free-energy calculations employed in the present work, the bond order parameters-based classification algorithm that identifies LP clusters, and deeper analysis on the 5-fold symmetric clusters and their topology during a spontaneous nucleation event (PDF)

Movie showing a spontaneous nucleation event (AVI)

AUTHOR INFORMATION

Corresponding Author

Gabriele M. Coli − *Soft Condensed Matter, Debye Institute for Nanomaterials Science, Department of Physics, Utrecht University, Utrecht 3584 CC, The Netherlands;* orcid.org/0000-0002-5125-8007; Email: g.m.coli@uu.nl

Authors

Tonnishtha Dasgupta − *Soft Condensed Matter, Debye Institute for Nanomaterials Science, Department of Physics, Utrecht University, Utrecht 3584 CC, The Netherlands*

Marjolein Dijkstra − *Soft Condensed Matter, Debye Institute for Nanomaterials Science, Department of Physics, Utrecht University, Utrecht 3584 CC, The Netherlands*

Complete contact information is available at: https://pubs.acs.org/10.1021/acsnano.9b07090

Author Contributions

‡T. Dasgupta and G. M. Coli contributed equally to this work.

Author Contributions

M.D. initiated the project on the role of softness in LP nucleation in binary nearly hard spheres and supervised T.D. and G.M.C. T.D. performed free-energy calculations and computed the thermodynamic phase diagram. G.M.C. determined the cluster criterion that distinguishes crystalline clusters with the Laves phase symmetry and calculated the degree of 5-fold symmetry in the binary fluid as a function of softness and supersaturation. G.M.C. and T.D. determined the nucleation free-energy barrier, nucleation rate, and kinetic glass transition and established thermodynamic and structural invariance for different degrees of softness, using MC and MD simulations, respectively. All authors cowrote the manuscript and analyzed and discussed the interpretation of the results.

Notes

The authors declare no competing financial interest.

ACKNOWLEDGMENTS

T.D. and M.D. acknowledge financial support from the Industrial Partnership Programme, "Computational Sciences for Energy Research" (Grant No. 13CSER025), of The Netherlands Organization for Scientific Research (NWO), which was cofinanced by Shell Global Solutions International B.V. G.M.C. was also financially supported by NWO (Grant No. 16DDS003).

REFERENCES

(1) Kalsin, A. M.; Fialkowski, M.; Paszewski, M.; Smoukov, S. K.; Bishop, K. J.; Grzybowski, B. A. Electrostatic Self-Assembly of Binary Nanoparticle Crystals with a Diamond-Like Lattice. *Science* **2006**, *312*, 420−424.

(2) Bishop, K. J.; Chevalier, N. R.; Grzybowski, B. A. When and Why Like-Sized, Oppositely Charged Particles Assemble into Diamond-Like Crystals. *J. Phys. Chem. Lett.* **2013**, *4*, 1507−1511.

(3) Shevchenko, E. V.; Talapin, D. V.; Kotov, N. A.; O'brien, S.; Murray, C. B. Structural Diversity in Binary Nanoparticle Superlattices. *Nature* **2006**, *439*, 55.

(4) Evers, W. H.; Nijs, B. D.; Filion, L.; Castillo, S.; Dijkstra, M.; Vanmaekelbergh, D. Entropy-Driven Formation of Binary Semiconductor-Nanocrystal Superlattices. *Nano Lett.* **2010**, *10*, 4235−4241.

(5) Yoshimura, S.; Hachisu, S. *Frontiers in Colloid Science In Memoriam Professor Dr. Bun-ichi Tamamushi*; Springer: New York, 1983; pp 59−70.

(6) Hasaka, M.; Nakashima, H.; Oki, K. Structure of the Laves Phase Observed in Polystyrene Latexes. *Trans. Jpn. Inst. Met.* **1984**, *25*, 65−72.

(7) Ma, G. H.; Fukutomi, T.; Morone, N. Preparation and Analysis of Ordered Structure of Binary Mixtures Composed of Poly (4-Vinylpyridine) and Polystyrene Microgels. *J. Colloid Interface Sci.* **1994**, *168*, 393−401.

(8) Gauthier, J.-P.; Fritsch, E.; Aguilar-Reyes, B.; Barreau, A.; Lasnier, B. Phase de Laves dans la Première Opale CT Bidisperse. *C. R. Geosci.* **2004**, *336*, 187−196.

(9) Cabane, B.; Li, J.; Artzner, F.; Botet, R.; Labbez, C.; Bareigts, G.; Sztucki, M.; Goehring, L. Hiding in Plain View: Colloidal Self-Assembly from Polydisperse Populations. *Phys. Rev. Lett.* **2016**, *116*, 208001.

(10) Schaertl, N.; Botin, D.; Palberg, T.; Bartsch, E. Formation of Laves Phases in Buoyancy Matched Hard Sphere Suspensions. *Soft Matter* **2018**, *14*, 5130−5139.

(11) Hynninen, A.-P.; Thijssen, J. H.; Vermolen, E. C.; Dijkstra, M.; Van Blaaderen, A. Self-Assembly Route for Photonic Crystals with a Bandgap in the Visible Region. *Nat. Mater.* **2007**, *6*, 202.

(12) Bommineni, P. K.; Klement, M.; Engel, M. *Growing Binary Hard Sphere Crystals. 2019*, arXiv:1912.06251. https://arxiv.org/pdf/1912.06251.pdf (accessed January 22, 2020).

(13) Jungblut, S.; Dellago, C. Crystallization of a Binary Lennard-Jones Mixture. *J. Chem. Phys.* **2011**, *134*, 104501.

(14) Zhao, K.; Mason, T. G. Shape-Designed Frustration by Local Polymorphism in a Near-Equilibrium Colloidal Glass. *Proc. Natl. Acad. Sci. U. S. A.* **2015**, *112*, 12063−12068.

(15) Ronceray, P.; Harrowell, P. Suppression of Crystalline Fluctuations by Competing Structures in a Supercooled Liquid. *Phys. Rev. E: Stat. Phys., Plasmas, Fluids, Relat. Interdiscip. Top.* **2017**, *96*, 042602.

(16) Russo, J.; Romano, F.; Tanaka, H. Glass Forming Ability in Systems with Competing Orderings. *Phys. Rev. X* **2018**, *8*, 021040.

(17) Teich, E. G.; van Anders, G.; Glotzer, S. C. Identity Crisis in Alchemical Space Drives the Entropic Colloidal Glass Transition. *Nat. Commun.* **2019**, *10*, 1−10.

(18) Frank, F. C. Supercooling of Liquids. *Proc. R. Soc. London A* **1952**, *215*, 43−46.

(19) Weeks, J. D.; Chandler, D.; Andersen, H. C. Role of Repulsive Forces in Determining the Equilibrium Structure of Simple Liquids. *J. Chem. Phys.* **1971**, *54*, 5237−5247.

(20) Wang, D.; Dasgupta, T.; van der Wee, E. B.; Zanaga, D.; Altantzis, T.; Wu, Y.; Coli, G. M.; Murray, C. B.; Bals, S.; Dijkstra, M.; van Blaaderen, A. *Binary Icosahedral Quasicrystals of Hard Spheres in*

Spherical Confinement. 2019, arXiv:1906.10088. https://arxiv.org/pdf/1906.10088.pdf (accessed January 24, 2020).
(21) Kawasaki, T.; Tanaka, H. Formation of a Crystal Nucleus from Liquid. *Proc. Natl. Acad. Sci. U. S. A.* **2010**, *107*, 14036−14041.
(22) Filion, L.; Ni, R.; Frenkel, D.; Dijkstra, M. Simulation of Nucleation in Almost Hard-Sphere Colloids: The Discrepancy between Experiment and Simulation Persists. *J. Chem. Phys.* **2011**, *134*, 134901.
(23) Richard, D.; Speck, T. Crystallization of Hard Spheres Revisited. I. Extracting Kinetics and Free Energy Landscape from Forward Flux Sampling. *J. Chem. Phys.* **2018**, *148*, 124110.
(24) Richard, D.; Speck, T. Crystallization of Hard Spheres Revisited. II. Thermodynamic Modeling, Nucleation Work, and the Surface of Tension. *J. Chem. Phys.* **2018**, *148*, 224102.
(25) Malins, A.; Williams, S. R.; Eggers, J.; Royall, C. P. Identification of Structure in Condensed Matter with the Topological Cluster Classification. *J. Chem. Phys.* **2013**, *139*, 234506.
(26) Taffs, J.; Royall, C. P. The Role of Fivefold Symmetry in Suppressing Crystallization. *Nat. Commun.* **2016**, *7*, 13225.
(27) Wood, N.; Russo, J.; Turci, F.; Royall, C. P. Coupling of Sedimentation and Liquid Structure: Influence an Hard Sphere Nucleation. *J. Chem. Phys.* **2018**, *149*, 204506.
(28) Crowther, P.; Turci, F.; Royall, C. P. The Nature of Geometric Frustration in the Kob-Andersen Mixture. *J. Chem. Phys.* **2015**, *143*, 044503.
(29) Espinosa, J. R.; Vega, C.; Valeriani, C.; Sanz, E. Seeding Approach to Crystal Nucleation. *J. Chem. Phys.* **2016**, *144*, 034501.
(30) Espinosa, J. R.; Sampedro, P.; Valeriani, C.; Vega, C.; Sanz, E. Lattice Mold Technique for the Calculation of Crystal Nucleation Rates. *Faraday Discuss.* **2016**, *195*, 569−582.
(31) Auer, S.; Frenkel, D. Crystallization of Weakly Charged Colloidal Spheres: A Numerical Study. *J. Phys.: Condens. Matter* **2002**, *14*, 7667−7680.
(32) Hansen, J.-P.; McDonald, I. R. *Theory of Simple Liquids*, second ed.; Elsevier: Cambridge, MA, 1990.
(33) Rosenfeld, Y.; Ashcroft, N. Theory of Simple Classical Fluids: Universality in the Short-Range Structure. *Phys. Rev. A: At., Mol., Opt. Phys.* **1979**, *20*, 1208.
(34) Ross, M. Generalized Lindemann Melting Law. *Phys. Rev.* **1969**, *184*, 233.
(35) Pedersen, U. R.; Costigliola, L.; Bailey, N. P.; Schrøder, T. B.; Dyre, J. C. Thermodynamics of Freezing and Melting. *Nat. Commun.* **2016**, *7*, 12386.
(36) Richard, D.; Speck, T. The Role of Shear in Crystallization Kinetics: From Suppression to Enhancement. *Sci. Rep.* **2015**, *5*, 14610.
(37) Barker, J. A.; Henderson, D. Perturbation Theory and Equation of State for Fluids. II. A Successful Theory of Liquids. *J. Chem. Phys.* **1967**, *47*, 4714−4721.
(38) Andersen, H. C.; Weeks, J. D.; Chandler, D. Relationship between the Hard-Sphere Fluid and Fluids with Realistic Repulsive Forces. *Phys. Rev. A: At., Mol., Opt. Phys.* **1971**, *4*, 1597.
(39) Götze, W. Recent Tests of the Mode-Coupling Theory for Glassy Dynamics. *J. Phys.: Condens. Matter* **1999**, *11*, A1.
(40) Brambilla, G.; El Masri, D.; Pierno, M.; Berthier, L.; Cipelletti, L.; Petekidis, G.; Schofield, A. B. Probing the Equilibrium Dynamics of Colloidal Hard Spheres above the Mode-Coupling Glass Transition. *Phys. Rev. Lett.* **2009**, *102*, 085703.
(41) Ni, R.; Stuart, M. A. C.; Dijkstra, M. Pushing the Glass Transition towards Random Close Packing Using Self-Propelled Hard Spheres. *Nat. Commun.* **2013**, *4*, 2704.
(42) Royall, C. P.; Malins, A.; Dunleavy, A. J.; Pinney, R. Strong Geometric Frustration in Model Glassformers. *J. Non-Cryst. Solids* **2015**, *407*, 34−43.
(43) Lindquist, B. A.; Jadrich, R. B.; Truskett, T. M. Communication: From Close-Packed to Topologically Close-Packed: Formation of Laves Phases in Moderately Polydisperse Hard-Sphere Mixtures. *J. Chem. Phys.* **2018**, *148*, 191101.
(44) Bommineni, P. K.; Varela-Rosales, N. R.; Klement, M.; Engel, M. Complex Crystals from Size-Disperse Spheres. *Phys. Rev. Lett.* **2019**, *122*, 128005.
(45) Avvisati, G.; Dasgupta, T.; Dijkstra, M. Fabrication of Colloidal Laves Phases *via* Hard Tetramers and Hard Spheres: Bulk Phase Diagram and Sedimentation Behavior. *ACS Nano* **2017**, *11*, 7702−7709.
(46) Ducrot, É.; He, M.; Yi, G.-R.; Pine, D. J. Colloidal Alloys with Preassembled Clusters and Spheres. *Nat. Mater.* **2017**, *16*, 652.
(47) Mattsson, J.; Wyss, H. M.; Fernandez-Nieves, A.; Miyazaki, K.; Hu, Z.; Reichman, D. R.; Weitz, D. A. Soft Colloids Make Strong Glasses. *Nature* **2009**, *462*, 83−86.
(48) Sengupta, S.; Vasconcelos, F.; Affouard, F.; Sastry, S. Dependence of the Fragility of a Glass Former on the Softness of Interparticle Interactions. *J. Chem. Phys.* **2011**, *135*, 194503.
(49) Krausser, J.; Samwer, K. H.; Zaccone, A. Interatomic Repulsion Softness Directly Controls the Fragility of Supercooled Metallic Melts. *Proc. Natl. Acad. Sci. U. S. A.* **2015**, *112*, 13762−13767.
(50) Pueblo, C. E.; Sun, M.; Kelton, K. Strength of the Repulsive Part of the Interatomic Potential Determines Fragility in Metallic Liquids. *Nat. Mater.* **2017**, *16*, 792−796.
(51) Anderson, J. A.; Lorenz, C. D.; Travesset, A. General Purpose Molecular Dynamics Simulations Fully Implemented on Graphics Processing Units. *J. Comput. Phys.* **2008**, *227*, 5342−5359.
(52) Glaser, J.; Nguyen, T. D.; Anderson, J. A.; Lui, P.; Spiga, F.; Millan, J. A.; Morse, D. C.; Glotzer, S. C. Strong Scaling of General-Purpose Molecular Dynamics Simulations on GPUs. *Comput. Phys. Commun.* **2015**, *192*, 97−107.
(53) Martyna, G. J.; Tobias, D. J.; Klein, M. L. Constant Pressure Molecular Dynamics Algorithms. *J. Chem. Phys.* **1994**, *101*, 4177−4189.

https://dx.doi.org/10.1021/acsnano.9b07090
ACS Nano 2020, 14, 3957−3968